World Academy of Science, Engineering and Technology
International Journal of Mechanical and Mechatronics Engineering
Vol:11, No:6, 2017

Unsteady Natural Convection Heat and Mass Transfer of Non-Newtonian Casson Fluid along a Vertical Wavy Surface

A. Mahdy, Sameh E. Ahmed

Abstract**—**Detailed numerical calculations are illustrated in our investigation for unsteady natural convection heat and mass transfer of non-Newtonian Casson fluid along a vertical wavy surface. The surface of the plate is kept at a constant temperature and uniform concentration. To transform the complex wavy surface to a flat plate, a simple coordinate transformation is employed. The resulting partial differential equations are solved using the fully implicit finite difference method with SUR procedure. Flow and heat transfer characteristics are investigated for a wide range of values of the Casson parameter, the dimensionless time parameter, the buoyancy ratio and the amplitude-wavelength parameter. It is found that, the variations of the Casson parameter have significant effects on the fluid motion, heat and mass transfer. Also, the maximum and minimum values of the local Nusselt and Sherwood numbers increase by increase either the Casson parameter or the buoyancy ratio.

Keywords**—**Casson fluid, wavy surface, mass transfer, transient analysis.

I. Introduction

NATURAL convection phenomena that generated by the simultaneous action of buoyancy forces obtaining from thermal and mass diffusion became very significant in nature and in a wide range of manufacturing applications in other words physics of the earth, oceanography, desiccation operation, chemical engineering and solidification of binary alloy. Several contributions that focused on combined heat and mass transfer in free convection boundary-layer flow along heated plates with unlike geometries is illustrated in the monograph by Gebhart el al. [1]. In addition, many researches have been carried out to include various physical aspects of the problem of combined heat and mass transfer from an irregular surface because irregular surfaces are often present in many applications and it is often encountered in heat devices to enhance heat transfer [2]-[5].

On the other hand, different types of fluids of considerable interest in different branches of science, engineering, and technology for instance molten plastics, polymers, and slurries depict a non-Newtonian fluid behavior. In the past decades, plentiful attempts of applying boundary layer theory to non-Newtonian fluids have done. The theory makes great simplifications in the governing equations of motion and energy; as a consequence, the equations are much easier to solve. For various non-Newtonian fluid models, an enormous amount of work has been done. Their full discussion is beyond the scope of this paper. Therefore, some examples will be quoted briefly. Due to ever growing engineering applications, major attention focused on the non-Newtonian fluids boundary-layer flows. In order to obtain a thorough familiarity of non-Newtonian fluids and their variety of applications, it is requisite to examine their flow behaviors. Indeed, the non-Newtonian fluids mechanics exhibit a special challenge to mathematicians, physicists and engineers. The non-linearity can express itself in a variety of procedures in numerous fields, like bio-engineering, drilling operations and food processing. Furthermore, for obtaining a thorough cognition of non-Newtonian fluids and its different applications, it is needful to addresses their flow behaviors. Due to their application in manufacture and technology, a number of problems in fluid mechanics have enjoyed the awareness that has been accorded to the flow which comprises non-Newtonian fluids. As known, Navier–Stokes theorem is disadvantageous for such non-Newtonian fluids because of the complexity of these fluids, and more than one constitutive equation is need to exhibit all fluids properties. Number of non-Newtonian fluid types have been investigated. In the literature, the vast majority of non-Newtonian fluid types are treated with simple types like the power-law and grade two or three [6]-[10]. These simple fluid types have flaw that render to results not having accordance with fluid flows in the reality.

Another type of non-Newtonian fluid is knowen as Casson fluid. In the literature, the type of non-Newtonian Casson fluid type is sometimes stated to fit rheological data better than general viscoplastic paradigm for several materials [11], [12]. For instance of non-Newtonian Casson fluid involves jelly, tomato sauce, honey, soup and concentrated fruit juices, etc. In addition, human blood can be deald as Casson fluid. Because of the existance of some substances like, protein, fibrinogen and globulin in aqueous base plasma, human red blood cells can form a chainlike structure, known as aggregates or rouleaux. If the rouleaux behave like a plastic solid, then there exists a yield stress that can be specified with the constant yield stress in Casson's fluid [13]-[15]. Punctually the non-linear Casson's constitutive equation has been used to characterize the flow profiles of suspensions of pigments in lithographic varnishes used for preparation of printing inks [16] and silicon suspensions [17]. The relation of shear stress–shear rate that obtained by Casson satisfactorily characterizes the properties of a number of over a number of shear rates polymers [18]. Non-Newtonian Casson fluid can be known as

A. Mahdy and Sameh E. Ahmed are with the Mathematics Department, Faculty of Science, South Valley University, Qena, Egypt (e-mail: mahdy@svu.edu.eg, sameh_sci_math@yahoo.com).

a shear thinning liquid which is presumed to have an infinite viscosity when rate of shear vanishes, a yield stress below which no flow happens, and a zero viscosity at an infinite rate of shear [19]. The flow of non-Newtonian Casson fluid between two rotating cylinders analyzed by Eldabe and Salwa [20], and Boyd et al. [21] investigated the Casson fluid flow for the steady and oscillatory blood flow. The authors in this contribution investigated the flow of boundary layer due to stretching surface with mass transfer. We venture further in the regime of unsteady two-dimensional boundary layer flows of a non-Newtonian fluid over a vertical wavy plate. The type of Casson fluid is utilized to characterize the behavior of non-Newtonian fluid.

II. Mathematical Formulation

A two-dimensional unsteady laminar boundary layer flow of non-Newtonian fluids past semi-infinite symmetric body with a sinusoidal wavy plate having constant wall temperature has calculated numerically. Fig. 1 depicted the schematic diagram of the physical model of the problem, where the axis of symmetry is aligned with the oncoming uniform stream. In our case, it's choosen that the sinusoidal wavy plate is characterized by $y = \delta(x)$ where $\hat{\delta}(\hat{x})$ is an arbitrary geometry function and described by $\hat{\delta} = \hat{\alpha}\sin(2\pi\hat{x} / L)$, where $\hat{\alpha}$ is the non-dimensional amplitude of the wavy surface and L is the characteristic wavelength of the wavy surface. The surface of the plate is kept at a constant temperature T_w and uniform concentration C_w. In addition, the fluid oncoming to the surface has a constant temperature T_∞ and concentration C_∞. All fluid properties are constant except the density in the buoyancy force term. The model of Casson fluid is utilized to illustrate the non-Newtonian fluid behavior. On the other hand, the rheological equation of state for an isotropic and incompressible flow of a Casson fluid can be written as:

$$\sqrt[n]{\tau} = \sqrt[n]{\tau_0} + \mu\sqrt[n]{\dot{\gamma}}$$

or, as seen from Nakamura and Sawada [22]:

$$\tau_{ij} = 2\left(\mu_B + \left(\frac{P_y}{\sqrt{2\pi}}\right)^{1/n}\right)^n e_{ij}$$

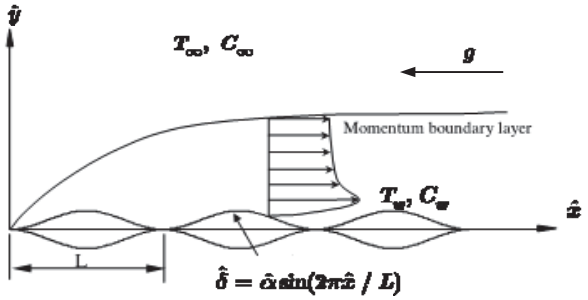

Fig. 1 Problem schematic and coordinate system

where μ is the dynamic viscosity, μ_B refers to plastic dynamic viscosity of the non-Newtonian fluid, P_y indicates the fluid yield stress, π represents the multipication of the component of rate of deformation with itself, that is, $\tau_{ij} = e_{ij}e_{ij}$, and e_{ij} symbolizes the (i,j)th component of the deformation rate. An anonymous referee has suggested to consider the value of $n = 1$. However, in many applications this value is $n \gg 1$. So, if a shear stress less than the yield stress is employed to the fluid, it behaves like a solid, whilst if a shear stress becomes greater than employed yield stress, it begins moving. Utilizing the balance laws of constitutive equation of mass, linear momentum energy and concentarion and with the help of Boussinesq's approximation the equations governing this flow can be re-written in the usual form as:

$$\frac{\partial\hat{u}}{\partial\hat{x}} + \frac{\partial\hat{v}}{\partial\hat{y}} = 0 \tag{1}$$

$$\frac{\partial\hat{u}}{\partial\hat{t}} + \hat{u}\frac{\partial\hat{u}}{\partial\hat{x}} + \hat{v}\frac{\partial\hat{u}}{\partial\hat{y}} = -\frac{1}{\rho}\frac{\partial\hat{P}}{\partial\hat{x}} + \nu\left(1+\frac{1}{\gamma}\right)\left(\frac{\partial^2\hat{u}}{\partial\hat{x}^2} + \frac{\partial^2\hat{u}}{\partial\hat{y}^2}\right) + g\beta(T-T_\infty) + g\tilde{\beta}(C-C_\infty) \tag{2}$$

$$\frac{\partial\hat{v}}{\partial\hat{t}} + \hat{u}\frac{\partial\hat{v}}{\partial\hat{x}} + \hat{v}\frac{\partial\hat{v}}{\partial\hat{y}} = -\frac{1}{\rho}\frac{\partial\hat{P}}{\partial\hat{y}} + \nu\left(1+\frac{1}{\gamma}\right)\left(\frac{\partial^2\hat{v}}{\partial\hat{x}^2} + \frac{\partial^2\hat{v}}{\partial\hat{y}^2}\right) \tag{3}$$

$$\frac{\partial T}{\partial\hat{t}} + \hat{u}\frac{\partial T}{\partial\hat{x}} + \hat{v}\frac{\partial T}{\partial\hat{y}} = \alpha^\star\left(\frac{\partial^2 T}{\partial\hat{x}^2} + \frac{\partial^2 T}{\partial\hat{y}^2}\right) \tag{4}$$

$$\frac{\partial C}{\partial\hat{t}} + \hat{u}\frac{\partial C}{\partial\hat{x}} + \hat{v}\frac{\partial C}{\partial\hat{y}} = D\left(\frac{\partial^2 C}{\partial\hat{x}^2} + \frac{\partial^2 C}{\partial\hat{y}^2}\right) \tag{5}$$

where, $(\hat{u},\hat{v})$ symbolize the velocity components in $(\hat{x},\hat{y})$ directions, respectively, ν is the kinematic viscosity, T,C are the temperature and concentration of the fluid inside the boundary layer, $\hat{P}$ represents the pressure, γ is the Casson parameter. $\beta,\tilde{\beta}$ refer to the thermal and concentration expansion coefficients, $\alpha^\star$ is the thermal diffusivity, g is the gravity, D indicates the mass diffusivity. Moreover, the appropriate boundary conditions for the governing equations are:

$$\hat{y} = \hat{\delta}, \quad \hat{u} = 0; \quad \hat{v} = 0; \quad T = T_w; \quad C = C_w \tag{6a}$$

$$\hat{y} \to \infty, \quad \hat{u} \to 0; \quad \hat{v} \to 0; \quad T \to T_\infty; \quad C \to C_\infty \tag{6b}$$

The initial step is to transform the irregular wavy surface into a flat surface by use of Prandtl's trans- position theorem, Yao [23]. In fact, the essence of that theory is that the flow is supplanted by the quantity of the perpendicular displacement of an asymmetrical solid plate, and the perpendicular component of the speed is regulated according to an inclination of the plate. The style of the boundary-layer equations doesn't change under the transformation, and the surface conditions can be considered on a transformed fiat surface. This lets the boundary conditions to be readily incorporated into any numerical method. Anyway, to

transform the governing equations, the following dimensionless quantities are introduced:

$$\overline{x}=\frac{\hat{x}}{L};\ \overline{y}=\frac{\hat{y}-\hat{\delta}}{L}Gr^{1/4};\ t=\frac{\nu\hat{t}}{L^2}Gr^{1/2},\ \overline{u}=\frac{L\hat{u}}{\nu Gr^{1/2}};$$
$$\overline{v}=\frac{L(\hat{v}-\delta'\hat{u})}{\nu Gr^{1/4}};\quad \theta=\frac{T-T_\infty}{T_w-T_\infty};\quad \phi=\frac{C-C_\infty}{C_w-C_\infty};\qquad (7)$$
$$\overline{P}=\frac{L^2}{\rho\nu^2Gr}\hat{P};\quad \delta'=\frac{d\hat{\delta}}{d\hat{x}}=\frac{d\overline{\delta}}{d\overline{x}};\quad \alpha=\frac{\hat{\alpha}}{L};\quad Gr=\frac{g\beta(T_w-T_\infty)L^3}{\nu^2}$$

Substituting (7) into (1)-(5) and ignoring the small order terms in Gr (i.e. let $Gr\to\infty$), we get the following ordinary governing differential equations:

$$\frac{\partial\overline{u}}{\partial\overline{x}}+\frac{\partial\overline{v}}{\partial\overline{y}}=0 \qquad (8)$$

$$\frac{\partial\overline{u}}{\partial t}+\overline{u}\frac{\partial\overline{u}}{\partial\overline{x}}+\overline{v}\frac{\partial\overline{u}}{\partial\overline{y}}=-\frac{\partial\overline{P}}{\partial\overline{x}}+\delta'\frac{\partial\overline{P}}{\partial\overline{y}}Gr^{1/4}+(1+\delta'^2)\left(1+\frac{1}{\gamma}\right)\frac{\partial^2\overline{u}}{\partial\overline{y}^2}+\theta+N\phi \qquad (9)$$

$$\frac{\partial\overline{v}}{\partial t}+\overline{u}^2\delta''+\delta'(\theta+N\phi)=\delta'\frac{\partial\overline{P}}{\partial\overline{x}}-(1+\delta'^2)\frac{\partial\overline{P}}{\partial\overline{y}}Gr^{1/4} \qquad (10)$$

$$\frac{\partial\theta}{\partial t}+\overline{u}\frac{\partial\theta}{\partial\overline{x}}+\overline{v}\frac{\partial\theta}{\partial\overline{y}}=\frac{1}{\mathrm{Pr}}(1+\delta'^2)\frac{\partial^2\theta}{\partial\overline{y}^2} \qquad (11)$$

$$\frac{\partial\phi}{\partial t}+\overline{u}\frac{\partial\phi}{\partial\overline{x}}+\overline{v}\frac{\partial\phi}{\partial\overline{y}}=\frac{1}{Sc}(1+\delta'^2)\frac{\partial^2\phi}{\partial\overline{y}^2} \qquad (12)$$

Parameters $Sc=\nu D^{-1}$, $N=\tilde{\beta}(C_w-C_\infty)/\beta(T_w-T_\infty)$ $\mathrm{Pr}=\nu\alpha^{-1}$ refer to Schmidt number, Buoyancy ratio parameter and Prandtl number. Anyway, it is obviously that when the parameter N has a nil value, the mass diffusion body force disappears and the problem reduces to pure heat convection; whereas as N tends to infinity, the thermal diffusion disappears. It is worth noting that the δ' and δ'' indicate the first and second differentiations of δ with respect to $\overline{x}$. For the problem under consideration the pressure gradient $\partial\overline{P}/\partial\overline{x}$ is zero. Therefore, eliminating $\partial\overline{P}/\partial\overline{y}$ in (9) and (10) resulting the following equation:

$$\frac{\partial\overline{u}}{\partial t}+\overline{u}\frac{\partial\overline{u}}{\partial\overline{x}}+\overline{v}\frac{\partial\overline{u}}{\partial\overline{y}}=(1+\delta'^2)\left(1+\frac{1}{\gamma}\right)\frac{\partial^2\overline{u}}{\partial\overline{y}^2}+\frac{1}{1+\delta'^2}\left(\theta+N\phi-\overline{u}^2\delta'\delta''\right) \qquad (13)$$

TABLE I
COMPARISON RESULTS OF LOCAL NUSSELT NUMBER AND LOCAL SKIN-FRICTION FOR NEWTONIAN FLUID ($\gamma\to\infty$)

Pr	Local Nusselt number		Local skin friction	
	Pullepu et al. [25]	Present	Pullepu et al. [25]	Present
0.001	0.0294	.0745331	1.4149	1.4019290
0.01	0.0797	.1018383	1.3356	1.3268480
0.1	0.2115	.2571416	1.0911	1.0282990
1	0.5125	.6113362	0.7668	.6480222

Applying the following transformation in order to remove the singularity at the leading edge [24]:

$$X=\overline{x};\ Y=\frac{\overline{y}}{(4\overline{x})^{1/4}};\ U=\frac{\overline{u}}{(4\overline{x})^{1/2}};\ V=(4\overline{x})^{1/4}\overline{v} \qquad (14)$$

Therefore, (8) and (11) up-to (13) in the parabolic coordinates (X,Y) become:

$$2U+4X\frac{\partial U}{\partial X}-Y\frac{\partial U}{\partial Y}+\frac{\partial V}{\partial Y}=0 \qquad (15)$$

$$\frac{\partial U}{\partial t}+4XU\frac{\partial U}{\partial X}+(V-YU)\frac{\partial U}{\partial Y}+\left(2+\frac{4X\delta'\delta''}{1+\delta'^2}\right)U^2=(1+\delta'^2)\left(1+\frac{1}{\gamma}\right)\frac{\partial^2U}{\partial Y^2}+\frac{1}{1+\delta'^2}(\theta+N\phi) \qquad (16)$$

$$\frac{\partial\theta}{\partial t}+4XU\frac{\partial\theta}{\partial X}+(V-YU)\frac{\partial\theta}{\partial Y}=\frac{1}{\mathrm{Pr}}(1+\delta'^2)\frac{\partial^2\theta}{\partial Y^2} \qquad (17)$$

$$\frac{\partial\phi}{\partial t}+4XU\frac{\partial\phi}{\partial X}+(V-YU)\frac{\partial\phi}{\partial Y}=\frac{1}{Sc}(1+\delta'^2)\frac{\partial^2\phi}{\partial Y^2} \qquad (18)$$

With the corresponding boundary conditions:

$$Y=0,\quad U=V=0;\quad \theta=1;\quad \phi=1 \qquad (19a)$$
$$Y\to\infty,\quad U\to0;\quad \theta\to0;\quad \phi\to0 \qquad (19b)$$

The computations of the local skin-friction coefficient, Nusselt number and Sherwood number are of practical interest. The local heat and mass transfer rates are large when the normal velocity is approaching the surface; they are small when the convective stream moves away from the surface. The heat and mass transfer mechanism along a wavy surface is different from that along a flat surface, and is modified by the fluid motion normal to the surface. The local Nusselt number and Sherwood number are defined respectively as:

$$Nu=\frac{h\hat{x}}{k}=-\left(\frac{Gr}{4X}\right)^{1/4}\sqrt{1+\delta'^2}\left(\frac{\partial\theta}{\partial Y}\right)_{Y=0} \qquad (20)$$

$$Sh=\frac{\tilde{h}\hat{x}}{D}=-\left(\frac{Gr}{4X}\right)^{1/4}\sqrt{1+\delta'^2}\left(\frac{\partial\phi}{\partial Y}\right)_{Y=0} \qquad (21)$$

In addition, the shearing stress on the wavy surface is:

$$\tau_w=\mu\left(1+\frac{1}{\gamma}\right)\left(\frac{\partial\hat{u}}{\partial\hat{y}}+\frac{\partial\hat{v}}{\partial\hat{x}}\right)_{\hat{y}=\delta} \qquad (22)$$

Since the local skin-friction coefficient C_{fx} is defined by:

$$C_{fx}=\frac{2\tau_w}{\rho\tilde{U}^2} \qquad (23)$$

where $\tilde{U}(=\nu Gr^{1/2}/L)$ is a characteristic velocity. Substituting (22) into (23) in terms of the non-dimensional quantities, we obtain:

$$C_{fx}=2\left(1+\frac{1}{\gamma}\right)\left(\frac{4X}{Gr}\right)^{1/4}(1-\delta'^2)\left.\frac{\partial U}{\partial Y}\right|_{Y=0} \qquad (24)$$

III. NUMERICAL METHOD AND VALIDATION

The numerical procedure used to solve the governing equations (15)-(18) with the boundary conditions (19) is based

on the fully implicit finite difference method. The central difference approaches are used to approximate both of the first and second derivatives. To illustrate the details of this method let us take the heat equation treatment (17) as an example. The finite difference form for this equation can be written as follows:

$$\frac{\theta_{l,k}^{m+1}-\theta_{l,k}^{m}}{\triangle\tau}=\frac{1}{\mathrm{Pr}}\frac{\theta_{l,k+1}^{m+1}-2\theta_{l,k}^{m+1}+\theta_{l,k-1}^{m+1}}{(\triangle Y)^2}-4X_lU_{l,k}^{m}$$

$$\times\frac{\theta_{l+1,k}^{m+1}-\theta_{l-1,k}^{m+1}}{2\triangle X}-(V_{l,k}^{m}-U_{l,k}^{m}Y_k)\frac{\theta_{i,k+1}^{m+1}-\theta_{l,k-1}^{m+1}}{2\triangle Y} \quad (25)$$

This can be re-arranged as:

$$A\theta_{l,k}^{m+1}=A_0\theta_{l,k}^{m}+A_1\theta_{l+1,k}^{m+1}+A_2\theta_{l-1,k}^{m+1}+A_3\theta_{l,k+1}^{m+1}+A_4\theta_{l,k-1}^{m+1} \quad (26)$$

where $A_0=\frac{1}{\triangle\tau}$; $A_1=\frac{-2X_iU_{l,k}^{m}}{\triangle X}$; $A_2=\frac{2X_iU_{l,k}^{m}}{\triangle X}$;

$$A_3=\frac{1}{\mathrm{Pr}(\triangle Y)^2}-\frac{V_{l,k}^{m}-U_{l,k}^{m}Y_k}{2\triangle Y}, \quad (27)$$

$$A_4=\frac{1}{\mathrm{Pr}(\triangle Y)^2}+\frac{V_{l,k}^{m}-U_{l,k}^{m}Y_k}{2\triangle Y};\qquad A=\frac{1}{\triangle\tau}+\frac{2}{\mathrm{Pr}(\triangle Y)^2}$$

The successive under-relaxation (SUR) form for (26) can be written as follows:

$$A\epsilon^{-1}\theta_{l,k}^{m+1}=A_0\theta_{l,k}^{m}+A_1\theta_{l+1,k}^{m+1}+A_2\theta_{l-1,k}^{m+1}+A_3\theta_{l,k+1}^{m+1}+A_4\theta_{l,k-1}^{m+1}+A(1-\epsilon)\epsilon^{-1}\theta_{l,k}^{m} \quad (28)$$

In (25)-(28), l,k denote the location and m refers to the time step. The value of successive under-relaxation parameter ϵ is considered to be equal 0.1. The grid size (60x40) is found to be suitable, here and the time step $\triangle\tau = 10^{-5}$ is considered for all calculations. This procedure was found to be suitable and gave results close to those obtained by Pullepu et al. [25]. As we can see from Table I, the present method compares very well with Pullepu et al. [25].

IV. Results and Discussion

The obtained numerical results are discussed in this section. This physical phenomenon is investigated for a wide range of the controlling parameter.

The ranges of these parameters are: the Casson parameter ($\gamma = 1, 5, 10, \infty$) the dimensionless time parameter ($\tau = 0.05, 0.1, 0.5, 1.0$ steady state), the buoyancy ratio ($N = 0, 2, 4$) and the amplitude-wavelength parameter ($\alpha = 0.05, 0.1, 0.2$) In all the obtained results, the air mixture with various mass species is considered. Fig. 2 displays the contours of the horizontal velocity components, isotherms and isoconcentration for different values of the Casson parameter γ at $\mathrm{Pr} = 0.7$, $Sc = 1.3$, $N = 2$ and $\alpha = 0.1$ In fact the present wavy surface can be described by the nodes of the wavy surface which are at $X = 0.5, 1.0, 1.5, 2.0$ etc. and $X = 0.75, 1.75, 2.75$ and so on are the troughs, and $X = 0.25, 1.25, 2.25$ are the crests. It is observed that, for the low values of γ the velocity component is represented by eight circular cells formed at troughs and crests in the region $0 \le Y \le 1.0$ and $0 \le X \le 4.0$ while there are blanks appears at the nodes of the wavy surface. In the remaining parts of the surface, the velocity changes periodically during the X-axis. On the other hand, the temperature and concentration profiles change periodically inside the whole flow domain.

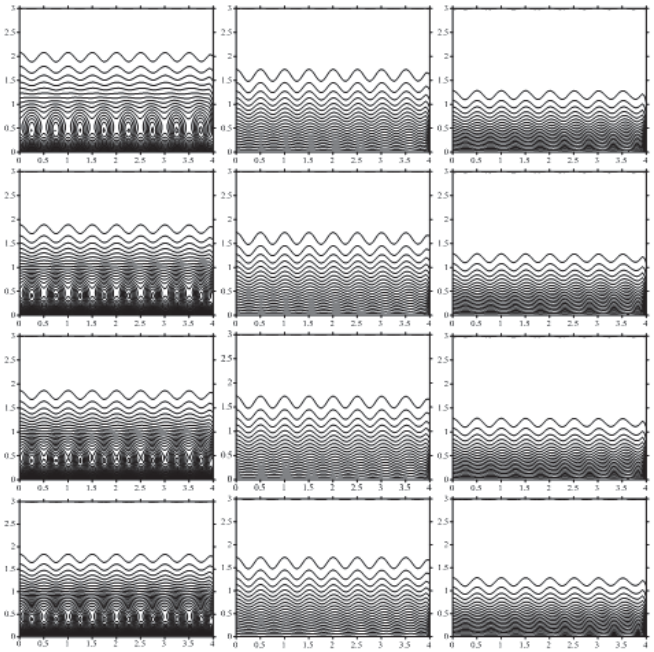

Fig. 2 Contours of U (*left*), θ (*middle*) and ϕ (*right*) at $\mathrm{Pr} = 0.7$, $Sc = 1.3$, $N = 2$, $\alpha = 0.1$ with $\gamma = 1, 5, 10, \infty$ (*From top to bottom*)

An increase in the Casson parameter γ causes a reduction in the fluid motion. This is evident from the small stretch of cells formed in the region $0 \le Y \le 1.0$ and $0 \le X \le 4.0$. Distributions of temperature and concentration have no noticeable change during changing the values of γ. The steady profiles of local skin-friction coefficient, local Nusselt number and Sherwood number for different values of γ at $X = 2.0$, $\mathrm{Pr} = 0.7$, $Sc = 1.3$ $N = 2$ and $\alpha = 0.1$ are depicted in Fig. 3. It is clear that, the increase in γ leads to a decrease in the skin friction coefficient. In addition, the reduction in distributions of temperature and concentration, previously referred because of the increased in γ resulting in an increase in temperature and concentration gradients, leading to enhancement the heat and mass transfer rates.

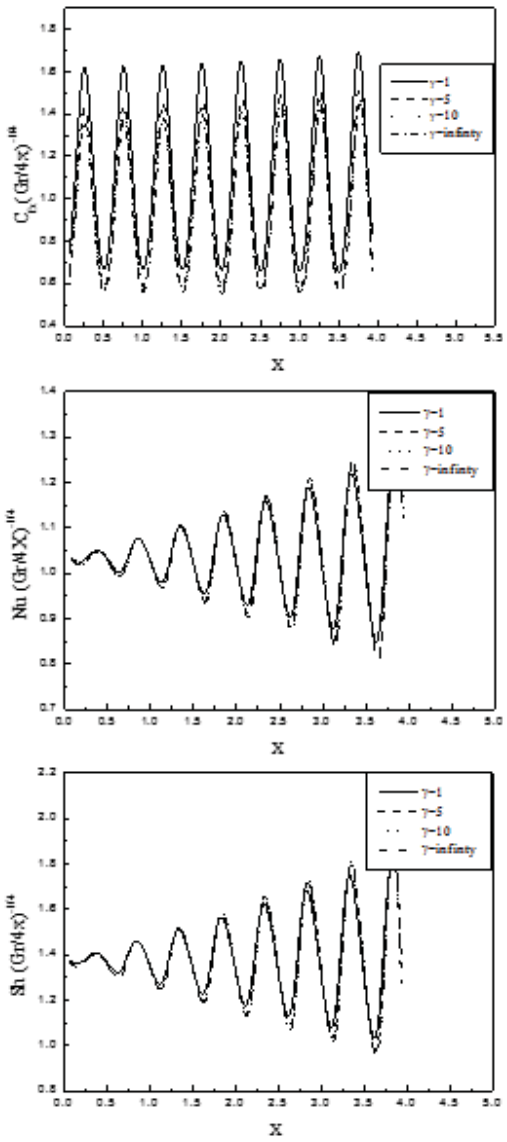

Fig. 3 Steady profiles of a) local skin-friction coefficient b) local Nusselt number c) Sherwood number for different values of γ at $X = 2$, $\mathrm{Pr} = 0.7$, $Sc = 1.3$, $N = 2$, $\alpha = 0.1$

Fig. 4 shows the contours of U, θ and ϕ for different values of the dimensionless time parameter at $\mathrm{Pr} = 0.7$, $Sc = 1.3$, $N = 2$, $\gamma = 0.1$ and $\alpha = 0.1$. As expected, at beginning of the simulation ($\tau = 0.05$), a little natural convection is obtained and the fluid motion is limited to the region $0 \le Y \le 0.8$ and $0 \le X \le 4.0$. Also, the contours of temperature and concentration are confined in the region $0 \le Y \le 0.5$ and $0 \le X \le 4.0$. As the time procedure, the natural convection increases and the contours of U start to occupy the flow domain. It is worth noting, here, that the steady state corresponds the value $\tau = 1.97$. The isotherms and isoconcentration distributions take the same behaviors of U as τ increases. Fig. 5 displays the profiles of local skin-friction coefficient, local Nusselt number and the Sherwood number for different values of τ at $\mathrm{Pr} = 0.7$, $Sc = 1.3$, $N = 2$, $\gamma = 0.1$ and $\alpha = 0.1$. It is noted that, the local skin friction increases monotonically as τ increases until take fixed values at the steady. However, the local Nusselt number and Sherwood number decrease clearly as τ increases. In this study, the buoyancy ratio parameter N is found to has significant effects on the fluid motion, heat and mass transfer. These effects are shown in Figs. 6 and 7. The referenced case for these figures is $\mathrm{Pr} = 0.7$, $Sc = 1.3$, $\gamma = 1$, and $\alpha = 0.1$.

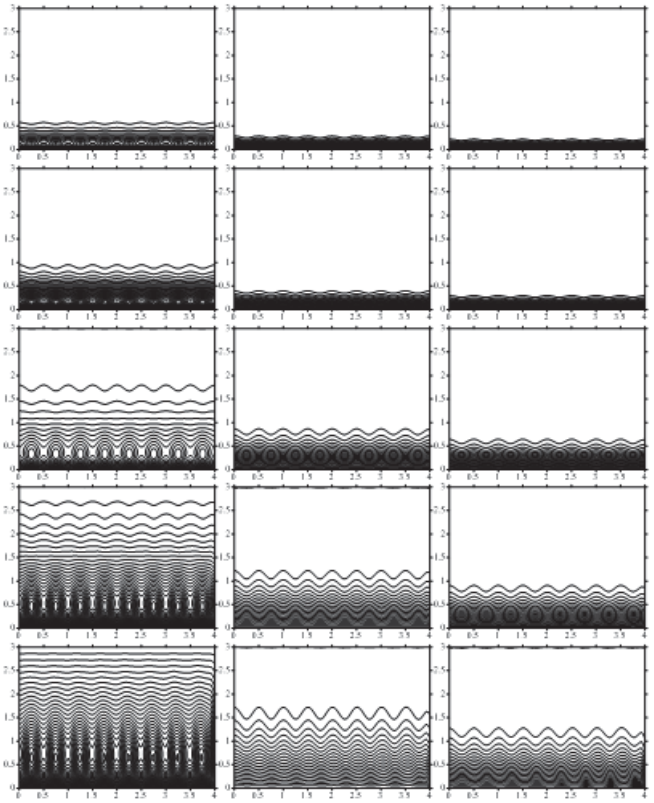

Fig. 4 Contours of U (*left*), θ (*middle*) and ϕ (*right*) at $\mathrm{Pr} = 0.7$, $Sc = 1.3$, $N = 2$, $\gamma = \alpha = 0.1$ with $\tau = 0.1, 0.5, 1.0$ (1.97 steady state) (*From top to bottom*)

An increase in the value of buoyancy ratio parameter N leads to increase both of the velocity distribution and local skin friction coefficient. On the other hand, the buoyancy ratio has not any clear effect on the isotherms and isoconcentration contours. But, the clear effects on the heat and mass characteristics appear in the behaviors of local Nusselt and Sherwood numbers. Fig. 7 shows that, there is considerable support in the rates of heat and mass transfer rates by increase the buoyancy ratio. There are interesting behaviors shown in Figs.8 and 9. These figures display the effects of the amplitude-wavelength parameter on the streamlines, isotherms and isoconcentration contours when $\mathrm{Pr} = 0.7$, $Sc = 1.3$, $\gamma = 0.5$, $N = 2$. Again, the fluid flow represented by eight

circular cells formed inside the region $0 \le Y \le 0.8$ and $0 \le X \le 4.0$, for the low values of α. Increasing in α causes an increase in the extension of these cells until take an egg-shape at $\alpha = 0.2$.

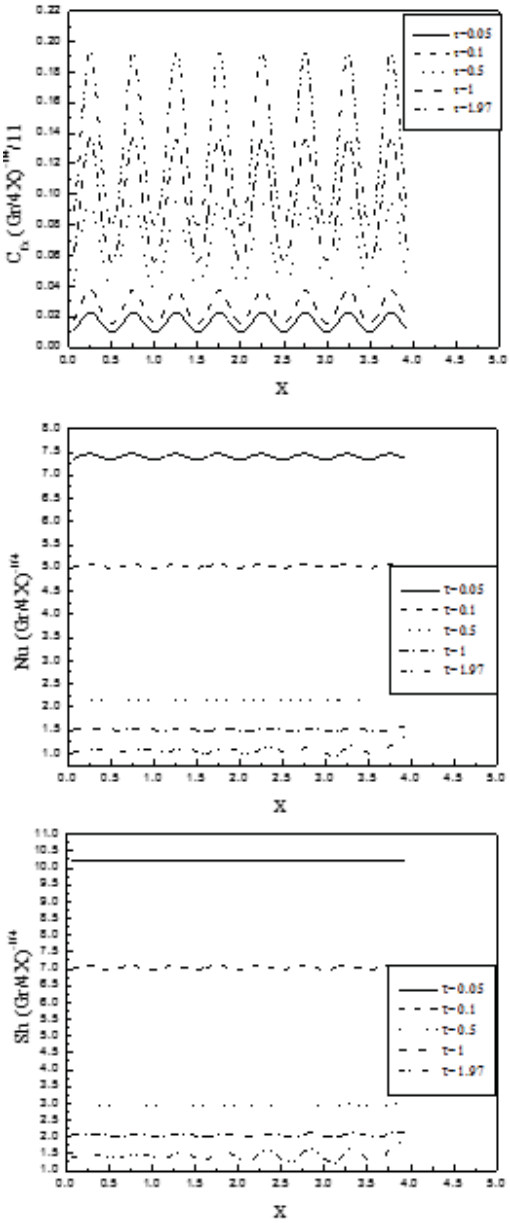

Fig. 5 Profiles of (a) local skin-friction coefficient (b) local Nusselt number (c) Sherwood number for different values of τ at $\mathbf{Pr} = 0.7$, $Sc = 1.3$, $N = 2$, $\gamma = \alpha = 0.1$

At the region $2.5 \le Y \le 3.0$ and $0 \le X \le 4.0$, the fluid flow takes a wave-like behavior which its amplitude increases as α increases. Regarding the isotherms and isoconcentration, these lines take the wave shape through the whole domain. The increase in amplitude-wavelength parameter α results in an increase in the amplitude of this shape. Fig. 9 displays the steady profiles of local skin-friction coefficient for different values of α at $\mathbf{Pr} = 0.7$, $Sc = 1.3$, $\gamma = 1$, $N = 2$ and $\alpha = 0.1$. It observed that, the skin-friction coefficient has a minimum value on the nodes (e.g., $X = 0.5, 1.0, 1.5, 2.0$, etc.). An increase in the parameter α leads to decrease the minimum values of the local skin friction coefficient. However, the maximum values of the local skin friction are the same for all values of α.

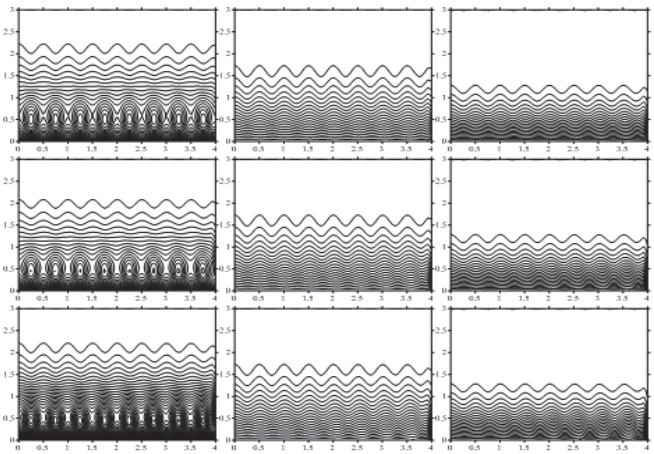

Fig. 6 Contours of U (*left*), θ (*middle*) and ϕ (*right*) at $\mathbf{Pr} = 0.7$, $Sc = 1.3$, $N = 2$, $\gamma = 1$, $\alpha = 0.1$ with $N = 0, 2, 4$ (*From top to bottom*)

V. Conclusions

The problem of unsteady natural convection heat and mass transfer of non-Newtonian Casson fluid along a vertical wavy surface was studied in this paper. The governing equations were transformed to a dimensionless form using a suitable transformation. The singularity at the leading edge was removed by introducing the new independent and dependent variables as functions in X and old variables. The resulting system was solved numerically using the fully implicit finite difference method. From this investigation, we can have concluded that, the increase in the Casson parameter leads to decrease the velocity and increases the maximum and minimum values of the local Nusselt number and the local Sherwood number. The behavior of the local skin friction increases slightly as the bouncy ratio parameter increases. The increase in the amplitude-wavelength parameter leads to decrease the minimum values of the local skin friction coefficient. However, the maximum values of the local skin friction are the same for all values of the amplitude-wavelength parameter.

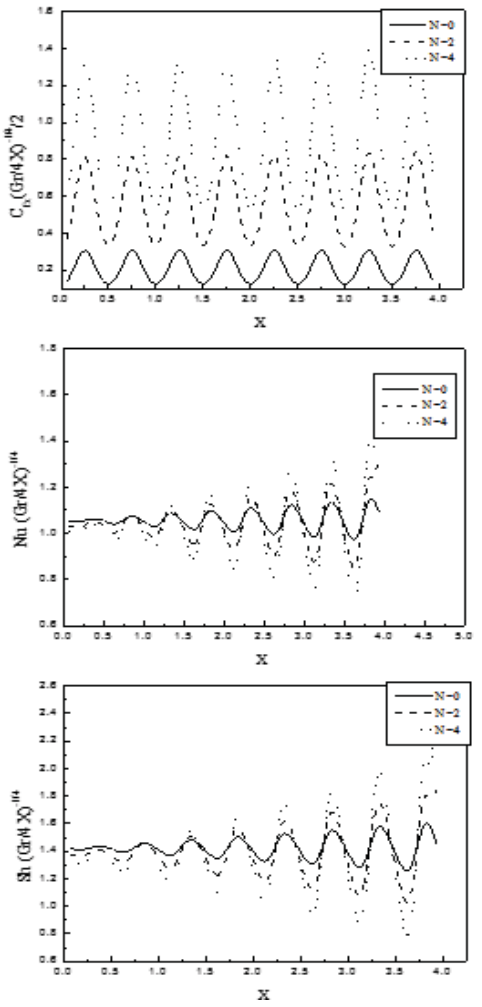

Fig. 7 Steady profiles of a) local skin-friction coefficient, b) local Nusselt number c) Sherwood number for different values of N at $\mathbf{Pr} = 0.7,\ Sc = 1.3, \gamma = 1,\ \alpha = 0.1$

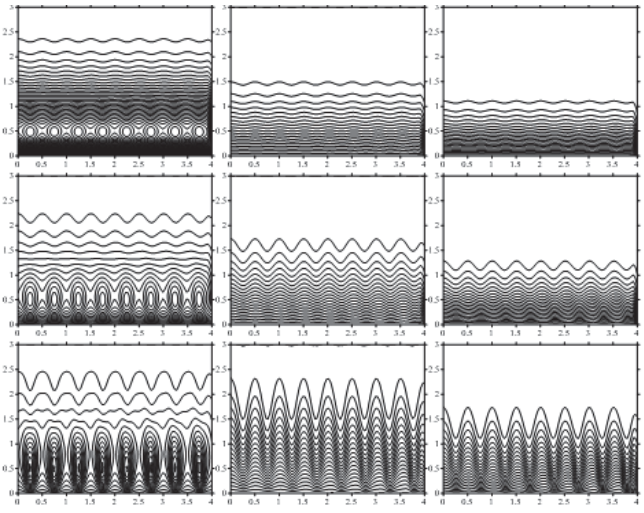

Fig. 8 Contours of U (*left*), θ (*middle*) and ϕ (*right*) at $\mathbf{Pr} = 0.7,\ Sc = 1.3,\ N = 2,\ \gamma = 0.5,\ \alpha = 0.1$ with $\alpha = 0.05, 0.1, 0.2$ (*From top to bottom*)

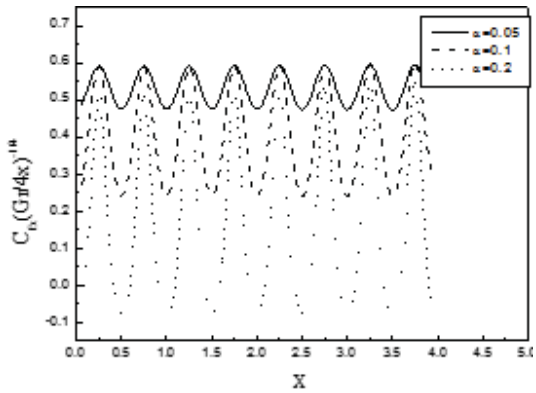

Fig. 9 Steady profiles of local skin-friction coefficient for different values of α at $\mathbf{Pr} = 0.7,\ Sc = 1.3,\ N = 2,\ \gamma = 1$

REFERENCES

[1] B.Gebhart, Y. Jaluria, R.L. Mahajan, B. Sammakia, *Buoyancy-Induced Flow and Transport*, Hemisphere, New York, 1998.

[2] J. Jer-Huan,Y. Wei-Mon, L. Hui-Chung, "Natural convection heat and mass transfer along a vertical wavy surface", *Int. J. Heat Mass Transfer* vol. 46 pp. 1075-1083, 2003.

[3] A. Mahdy, "MHD non-Darcian free convection from a vertical wavy surface embedded in porous media in the presence of Soret and Dufour effect", *Int. Commu. Heat Mass Transfer,* vol. 36, pp. 1067-1074, 2009.

[4] A. Mahdy, E.A. Sameh, Laminar free convection over a vertical wavy surface embedded in a porous medium saturated with a nanofluid, *Transp. Porous Med.*, vol 91, pp. 423–435, 2012.

[5] E.A. Sameh, M.M. Abd El-Aziz, "Effect of local thermal non-equlibrium on unsteady heat transfer by natural convection of a nanofluid over a vertical wavy surface:, *Meccanica* vol. 48, pp. 33-43, 2013.

[6] H.I. Andersson and B.S. Dandapat, "Flow of a power-law fluid over a stretching sheet", *Appl. Anal. Continuous Media* vol. 1, pp. 339-347, 1992.

[7] I.A. Hassanien, "Flow and heat transfer on a continuous flat surface moving in a parallel free stream of power-law fluid", *Appl. Model* vol. 20 pp. 779–784, 1996.

[8] B. Serdar, M. Salih Dokuz, "Three-dimensional stagnation point flow of a second grade fluid towards a moving plate", *Int. J. Eng. Sci.* vol. 44, pp. 49–58, 2006.

[9] A.M. Siddiqui, A. Zeb, Q.K. Ghori, A.M. Benharbit, "Homotopy perturbation method for heat transfer flow of a third grade fluid between parallel plates", *Chaos Solitons Fractals* vol. 36, pp. 182–192, 2008.

[10] M. Sajid, I. Ahmad, T. Hayat and M. Ayub, "Unsteady flow and heat transfer of a second grade fluid over a stretching sheet", *Commun. Nonlinear Sci. Numer. Simul.* Vol. 14, pp. 96–108, (2009).

[11] M. Mustafa, T. Hayat, I. Pop and A. Aziz, "Unsteady boundary layer flow of a Casson fluid due to an impulsively started moving flat plate", *Heat Transfer – Asian Res.* Vol. 40, pp. 563–576, 2011.

[12] K. Bhattacharyya, T. Hayat, A. Alsaedi, "Analytic solution for magnetohydrodynamic boundary layer flow of Casson fluid over a stretching/shrinking sheet with wall mass transfer", *Chin. Phys. B* vol. 22(2), pp. 024702, 2013 .

[13] Y.C. Fung, *Biodynamics circulation*. New York Inc: Springer Verlag; 1984.

[14] S. Nadeem, R. Ul Haq, C. Lee, "MHD flow of a Casson fluid over an exponentially shrinking sheet", *Sci. Iran* vol. 19(6), pp. 1550–1553, (2012).

[15] A. Kandasamy, R.G. Pai, "Entrance region flow of Casson fluid in a circular tube", *Appl. Mech. Mater* vol. 110/116, pp. 698–706, (2012).

[16] N. Casson In: Mill CC, editor. *Rheology of dispersed system*, vol. 84. Oxford: Pergamon Press; 1959.

[17] W.P. Walwander, T.Y. Chen, D.F. Cala, Biorheology vol. 12, pp. 111, 1975.

[18] G.V. Vinogradov, A.Y. Malkin, *Rheology of polymers*. Moscow: Mir Publisher; 1979.

[19] R.K. Dash, K.N. Mehta and G. Jayaraman, "Casson fluid flow in a pipe filed with a homogeneous porous medium", *Int. J Eng. Sci.* vol. 34(10), pp. 1145–1156, 1996.
[20] N.T.M. Eldabe, M.G.E. Salwa, "Heat transfer of MHD non-Newtonian Casson fluid flow between two rotating cylinders", *J. Phys. Soc. Jpn*. Vol. 64, pp. 41–64, 1995.
[21] J. Boyd, J.M. Buick, S. Green, "Analysis of the Casson and Carreau-Yasuda non-Newtonian blood models in steady and oscillatory flow using the lattice Boltzmann method", *Phys. Fluids* vol. 19, pp. 93–103, 2007.
[22] M. Nakamura, T. Sawada, Numerical study on the flow of a non-Newtonian fluid through an axisymmetric stenosis, *ASME J Biomechanical Eng* vol. 110, pp. 137–143, 1988.
[23] L.S. Yao, "A note on Prandtl's transposition theorem", *ASME J. Heat Transfer* vol. 110, pp. 503-507, 1989.
[24] L.S. Yao, "Natural convection along a wavy surface", *ASME J. Heat Transfer* vol. 105, pp. 465-468, 1983.
[25] Bapuji Pullepu, Ali J. Chamkha,, I. Pop, "Unsteady laminar free convection flow past a non-isothermal vertical cone in the presence of a magnetic field", *Chem. Eng. Comm.*, vol. 199, pp. 354-367, 2012.